RESEARCH ARTICLE

Translational readthrough generates new astrocyte AQP4 isoforms that modulate supramolecular clustering, glial end feet localization, and water transport

Manuela De Bellis, Francesco Pisani, Maria Grazia Mola, Stefania Rosito, Laura Simone, Cinzia Buccoliero, Maria Trojano, Grazia Paola Nicchia, Maria Svelto, Antonio Frigeri.

https://doi.org/10.1002/glia.23126

Funding information: This study was financed by the Italian Ministry of University and Research (Project Firb "Futuro in Ricerca" RBFR12SJA8 to Grazia Paola Nicchia, by Apulian Region funding PON project 01_01297 to Antonio Frigeri and by PON project 02_00576 "AMIDHERA-Sistemi avanzati mini-invasivi di diagnosi e radioterapia" to Maria Svelto. Dr. Francesco Pisani is a research fellow of the Apulia region program "Future in research" (project n. 5CU9HC5).

Abstract

Regulation of water homeostasis is a central feature of central nervous system pathophysiology. In this context, several lines of evidence suggest a crucial role for the water channel aquaporin-4 (AQP4) and its plasma membrane supramolecular organization as the key element. Here, we demonstrate the expression in tissues of additional isoforms of AQP4 characterized by a C-terminal extension generated by programmed translational readthrough. These extended isoforms (AQP4ex) display a perivascular polarization and expression in dystrophin-dependent pools. AQP4ex reduces supramolecular clustering tendency and allows AQP4 interactions with syntrophin. Furthermore, site-directed mutagenesis of two serines in the extended C-terminus of AQP4ex showed potential regulation of water permeability by phosphorylation. Finally, AQP4ex expression can be positively modulated by gentamicin treatment, demonstrating the possibility of regulating the AQP4 translational readthrough frequency. This novel regulatory mechanism could have important pathophysiological implications for conditions in which alternations have been reported in AQP4 structure.

1 Introduction

AQP4 plays a pivotal role in the maintenance of body and cellular water homeostasis, and its expression is altered in several pathological states such as brain ischemia, tumors (Papadopoulos & Verkman, 2013), and neuromyelitis optica (NMO), an autoimmune demyelinating disease (Lennon, Kryzer, Pittock, Verkman, & Hinson, 2005; Nicchia et al., 2009). The regulation of AQP4 expression and/or function is a major issue in studies investigating the physiopathological role of this water channel. AQP4 expression and activity can be regulated either by short- or long-term mechanisms. Short-term regulation of AQP4 is based essentially on the control of protein activity via potential phosphorylation, although this conclusion remains debated (Han, Wax, & Patil, 1998; McCoy, Haas, & Sontheimer, 2010; Zelenina, Zelenin, Bondar, Brismar, & Aperia, 2002); otherwise, long-term regulation refers to transcriptional, posttranscriptional and translational control. To date, a complex mechanism of translational control of AQP4 has been described, suggesting that the regulation of AQP4 isoform expression, function and assembly in supramolecular structures, called orthogonal arrays of particles (OAPs), primarily occurs at the posttranscriptional level. Indeed, the ratio of the two major AQP4 isoforms (M1 and M23), which determinates the OAP size, is regulated by leaky scanning (LS) and reinitiating mechanisms, both of which are influenced by the 5'UTR sequence of AQP4 (Pisani, Rossi, Nicchia, Svelto, & Frigeri, 2011; Rossi, Pisani, Nicchia, Svelto, & Frigeri, 2010). Moreover, the most recently identified human AQP4 isoform, AQP4-Δ4, which is derived from alternative splicing of exon 4, exerts a dominant-negative effect on the full-length canonical protein, thus reducing its plasma membrane expression and water transport (De Bellis et al., 2014). Furthermore, the presence of other AQP4 isoforms has been reported in rats (Moe et al., 2008). The distinctive ratios of these AQP4 isoforms in different tissues expressing similar levels of AQP4 mRNA indicate that cells can regulate the expression of particular AQP4 isoforms according to their specific homeostatic needs. Furthermore, recent studies have suggested that tissue-related differences in AQP4-OAP assembly could be involved in the tissue specificity of NMO pathogenesis (Pisani et al., 2015). Just as LS and alternative splicing provide a means for a protein to acquire new N-terminal domains or functional modules, translational readthrough (TRT) can provide a mechanism for protein evolution at the C-terminus. The translation of mRNAs normally terminates at an in-frame stop codon. However, in a few circumstances, translation can continue beyond the stop codon to a downstream stop codon, generating a C-terminal polypeptide extension (Namy et al., 2003). Such TRT events are best understood in viruses (Li & Rice, 1989; Pelham, 1978), but they have also been well documented in bacteria (Jalajakumari & Manning, 1989), yeast (Namy et al., 2003), Drosophila (Dunn, Foo, Belletier, Gavis, & Weissman, 2013; Robinson & Cooley, 1997), and only very recently in mammalian genes (Eswarappa et al., 2014; Loughran et al., 2014; Schueren et al., 2014). TRT plays important regulatory roles and is functionally important in terms of changing the C-terminal sequence of a given protein, which may modulate its activity/stability and/or localization. Recently, TRT of VEGF-A has been reported to produce an extended isoform, VEGF-Ax, with antiangiogenic activity (Eswarappa et al., 2014), and the extended isoform of the lactate dehydrogenase enzyme displays a different localization and function compared with the cytosolic canonical isoform

(Schueren et al., 2014). Therefore, stop codon readthrough appears to be essential for modulating the function of regular-sized proteins in mammals.

Recently, two independent computational studies revealed that AQP4 mRNA could be a TRT candidate (Loughran et al., 2014; Schueren et al., 2014). A critical clue was offered by analysis of the 3'UTR sequence of the AQP4 mRNA. In humans, an in-frame, evolutionarily conserved UAA stop codon was observed 84 nucleotides downstream of the canonical AQP4 stop codon. The AQP4 UGA canonical stop codon and the CUAG motif immediately downstream of the stop codon are highly conserved throughout vertebrates and have been reported to be weak termination signals. Remarkably, the amino acid sequence, which is potentially encoded by the region between the stop codons, is likewise conserved in mammals, but the sequence beyond the downstream stop codon is weakly conserved. Based on these observations, it was hypothesized that AQP4 mRNA translation extended beyond the canonical stop codon and terminated at the downstream in-frame stop codon. This TRT event would generate a new AQP4 isoform containing a 29-amino acid C-terminal extension (including an amino acid replacement of the stop codon). Until now, whether AQP4 readthrough also occurs in vivo and the potential functional role of this new extended isoform has not been investigated.

Here, for the first time, we demonstrate that AQP4 mRNA undergoes robust TRT in human and rat tissues to generate AQP4ex with a 29-amino-acid C-terminal extension. Remarkably, the extended C-terminal tail in AQP4ex has a great impact on supramolecular AQP4 organization, water permeability and polarization throughout the interaction with α-syntrophin.

2 Material and methods

2.1 Human samples

Human samples were obtained from patients who underwent surgery (De Bellis et al., 2014). Informed consent was obtained from the patients. Depending on the size of the tissue, two portions of the tissue were obtained for immunofluorescence analysis and protein extraction. Human spinal cord biopsies were purchased from Abcam and processed as indicated by the company.

2.2 Animals

Experiments were performed in accord with the European directive on animal use for research and Italian law on animal care. This project has been approved by the Institutional Care and Use Committee of the University of Bari and by the Italian Health Department (Approved Project no. 100/2014-B). All experiments were designed to minimize the number of animals used and animal suffering. Wistar rats were maintained under a 12-h dark to light cycle, constant room temperature and humidity (22±2°C, 75%), with food and water provided ad libitum, and they supplied with environmental enrichment materials such as toys and shelters.

2.3 Antibodies

Anti-AQP4 was purchased from Santa Cruz Biotechnology (goat polyclonal immunoglobulin G) and diluted 1:400 for immunofluorescence and 1:500 for immunoblot analysis. Rabbit anti-actin (Sigma) was used for immunoblotting at 1:500. Rabbit anti-α syntrophin (Sigma) was used at 1:1,000 for immunofluorescence and immunoprecipitation experiments. Rabbit anti-AQP4ex (human specific) (a kind gift from Dr. Lounghran) was used at 1:400 for immunofluorescence and 1:1,000 for immunoblotting and immunoprecipitation experiments. An affinity-purified rabbit polyclonal antibody to a predicted antigen (DSTENRRDSLELAS) within the rat AQP4 carbossi extension was prepared by GenScript and diluted 1:400 for immunofluorescence and 1:1,000 for immunoblot analysis. The secondary antibodies used for Western blot included peroxidase-conjugated donkey anti-goat and goat anti-rabbit antibodies (Santa Cruz Biotechnology) diluted 1:5,000. The secondary antibodies used for immunofluorescence were Alexa Fluor 594 donkey anti-goat and Alexa Fluor 488 goat anti-human, donkey anti-rabbit and donkey anti-goat (Thermo) diluted 1:1,000.

2.4 Cloning of the AQP4ex 3'UTR and site-directed mutagenesis

One microgram of total human frontal cortex RNA (Clontech) was retro-transcribed using Super Script III reverse transcriptase (Invitrogen) as recommended by the manufacturer, and the obtained single-stranded cDNA was PCR-amplified using primers AQP4M1For, AQP4M23For, and AQP4ex3'UTRRev shown in Supporting Information Table S1. The PCR products were analyzed by electrophoresis in a 1% agarose gel in tris-acetate-EDTA (TAE) buffer. Subsequently, the selected PCR fragment of the expected size (1 kb) was cut from the agarose gel, purified using the Qiaex II gel extraction kit (Qiagen), and then cloned into pTarget Mammalian Expression Vector system (Promega). The human AQP4ex 3'UTR sequence cloned into pTarget was used as a template for single point mutation (AQP4ex, AQP4exAla, AQP4exAsp) using the QuickChange site-directed II kit (Stratagene) according to the manufacturer's instructions. All constructs were fully sequenced.

2.5 Cell cultures and transfection

Rat cortical astrocyte primary cultures were prepared as previously described (Nicchia, Frigeri, Liuzzi, & Svelto, 2003). HEK, U87MG, and astrocyte (DI TNC1) cell lines were maintained in Dulbecco's high-glucose medium (Invitrogen) supplemented with 10% fetal bovine serum (Invitrogen) and penicillin/streptomycin (Invitrogen). Six hours before transfection, the cells at 60 to 70% confluency were plated using antibiotic-free medium. The cells were transfected with Optifect (Invitrogen) according to the manufacturer's protocol and analyzed after 30 to 48 h.

2.6 Immunofluorescence

Ten-micron transverse sections of frozen tissues were prepared using a cryostat (CM 1900; Leica) and stored on positively charged glass slides (Thermo Scientific). The sections were fixed in 4% paraformaldehyde, washed with phosphate-buffered saline (PBS), blocked using 0.1% gelatin in PBS for 30 min at room temperature (rt), incubated at rt for 1 h with primary antibodies, washed with PBS-gelatin, and incubated with Alexa-conjugated secondary antibodies. DI TNC1 cells plated on

coverslips were fixed in 4% paraformaldehyde, washed with PBS, and permeabilized with 0.3% Triton X-100 in PBS. After blocking with 0.1% gelatin in PBS, the cells were incubated with primary antibodies for 1 h at room temperature. After washing in PBS, the cells were incubated with Alexa-conjugated secondary antibodies for 30 min. Confocal images were obtained using an automated inverted Leica TCS SP8 confocal microscope with a 20× and 63× HC PL Apo oil CS2 objective. In all experiments, no-primary and no-secondary antibody controls were run in parallel. In some experiments, to verify the specificity of the stain, an immunodepleted control was assessed. No specific staining was observed in these controls.

2.7 Gated stimulated emission depletion (gSTED) super resolution microscopy

Immunofluorescence for gSTED was performed as reported in the Quick Guide to the STED Sample Preparation (http://www.leica-microsystems.com). Briefly, the cells were washed with PBS (Euroclone), fixed with 2% PFA in PBS for 10' (Sigma), washed with PBS, permeabilized with 0.3% Triton X-100 (Sigma) for 10 min, saturated with 2% BSA (Sigma) in PBS, incubated with commercial anti-AQP4 antibody (Santa Cruz Biotechnology, goat polyclonal IgG) in 2% BSA in PBS, washed with 2% BSA in PBS, incubated with secondary anti-goat Alexa Fluor 488-conjugate (Thermo) in 2% BSA in PBS, washed with PBS, and finally mounted with Mowiol. For image acquisition and analysis, a Leica TCS SP8 STED 3× microscope and Leica LASX software were used (Leica Microsystems CMS GmbH). A Leica HC PL APO 100×/1.40 Oil STED White objective and Type F Immersion liquid with a refractive index of 1.5 were used. Excitation of the Alexa Fluor 488 dye was achieved with a continuous wave at 488 nm using a diode laser with a maxim light output in the focal plane of 10 mW (NKT Photonics supercontinuum laser). Depletion was performed using a fiber laser with continuous wave of 592 nm and a maxim light output in the focal plane of <0.5 mW (Laser Quantum). gSTED images were deconvoluted using Huygens Professional Software (Scientific Volume Imaging) and used to determine the aggregate size of AQP4. To determine the aggregate size of AQP4, random areas were selected from representative images, and an intensity profile was plotted for each aggregate using the "determine FWHM" function in the Leica LASX software. The width of the profile at half-maximal intensity was measured as the cluster size (Full Width at Half Maximum (FWHM) (Zuidscherwoude et al., 2015). At least one hundred clusters per area were measured.

2.8 Fluorescence-quenching assay for water transport measurements

Cells were seeded in 96-well black-walled microplates (Corning) then incubated at 37°C for 45 min with 10 μM membrane-permeable calcein-AM (Thermo). Changes in calcein fluorescence which are directly proportional to changes in the cell volume were recorded on a Flex Station3 (Molecular Devices) plate reader (Mola, Nicchia, Svelto, Spray, & Frigeri, 2009). The cells were rinsed in isotonic DPBS, and hypertonicity was applied 15s after the beginning of each reading via the addition of an appropriate volume of mannitol to achieve a final osmolarity of 450 mOsm. Time course fluorescence data following cell mixing with hyperosmotic solution were recorded over a 90s period. Data acquisition was performed using SoftMaxPro software, and the data were analyzed using Prism

(Graph Pad) software. The time constant of cell shrinkage was obtained by fitting the data to an exponential function.

2.9 AQP4 cRNA synthesis and *Xenopus laevis* water transport assay and immunofluorescence

X. laevis oocytes were surgically removed from anesthetized frogs (2 g/L of Tricaine; Sigma) and defolliculated as previously reported (Nicchia et al., 2011). The mMessage mMachine T7 in vitro transcription kit (Ambion) was used to produce cRNA from each construct for oocyte injection. Twenty nanograms of cRNAs were injected into single oocytes using an automated microinjector (Nanoject; Drum-mond Scientific), and P_f was measured (Nicchia et al., 2011). For immunofluorescence analysis of oocytes, 3 days after injection, they were fixed in 4% paraformaldehyde with 0.1 M sucrose for 4 h at room temperature, cryoprotected in 30% sucrose in PBS at 4°C overnight, mounted in OCT, and sectioned into 10 µm slices. Immunofluorescence was then performed using a commercial anti-AQP4 antibody at 1:500 (Santa Cruz Biotechnology, goat polyclonal IgG) and a secondary anti-goat Alexa Fluor 488 conjugate at 1:1,000 (Thermo). Immunostained oocytes slices were observed using a photomicroscope equipped for epifluorescence (DMRXA; Leica), and digital images were obtained with a DMX 1200 camera (Nikon).

2.10 Blue native-page (BN-PAGE) and 2DE

Twenty 10-µm thick cryosections of human tissues were dissolved in seven volumes of BN buffer (1% Triton X-100, 12 mM NaCl, 500 mM 6-aminohexanoic acid, 20 mM Bis-Tris, pH 7.0, 2 mM EDTA, 10% glycerol) plus Protease Inhibitor Cocktail (Roche). A confluent layer of transfected DI TNC1 cells was washed once with ice-cold PBS, harvested with a cell scraper, and lysed into seven volumes of BN buffer plus Protease Inhibitor Cocktail (Roche). The cells and tissues were lysed on ice for 1 h, and the samples were than centrifuged at 22,000 ×*g*for 30 min at 4°C. The supernatants were collected, and the total protein content was calculated using the BCA Protein Assay Kit (Thermo). Twenty micrograms of protein sample were mixed with 5% CBB G-250 (Coomassie blue G-250) and loaded onto a polyacrylamide native gradient gel (4–9%) (Schagger, Cramer, & von Jagow, 1994). The running buffers were as follows: anode buffer (25 mM imidazole, pH 7) and blue cathode buffer (50 mM tricine; 7.5 mM imidazole; 0.02% Coomassie blue G-250; pH 7). Electrophoresis was performed at 6 mA and stopped when the tracking line of the CCB G-250 dye had left the edge of the gel. Proteins were blotted onto polyvinylidene difluoride (PVDF) membranes (Millipore) for immunoblot analysis. For the 2D BN/SDS-PAGE analysis, lanes from the first dimension were cut into individual strips and equilibrated in denaturing buffer (1% SDS and 1% β-mercaptoethanol) for 1 h at rt and placed in a 2D SDS-PAGE with the same thickness. Separation of the second dimension was performed in a 13% SDS-polyacrylamide gel at 25 mA per gel. At the end of the run, the gel was blotted onto a PVDF membrane (Millipore) for Western blot analysis.

2.11 SDS-PAGE

2.11.1 Protein sample preparation for SDS-PAGE

Twenty 10-µm thick cryosections of human and rat tissues were dissolved in seven volumes of RIPA lysis buffer (10 mM Tris-HCl, pH 7.4, 140 mM NaCl, 1% Triton X-100, 1% Na deoxycholate, 0.1% SDS, 1× Protease Inhibitor Cocktail, 1 mM Na_3VO_4, 1 mM NaF, and 1 mM EDTA). Transfected HeLa cells and rat astrocytes were washed once in ice-cold phosphate-buffered saline (PBS) and dissolved in RIPA buffer. Cells and tissues lysates were then sonicated for 10 s on ice, and after a 30 min incubation on ice, the samples were centrifuged at 22,000 ×g for 30 min at 4°C. The supernatants were collected, and the protein concentration was determined using the BCA protein assay (Bio-Rad). Membrane proteins were dissolved in Laemmli Sample Buffer (Bio-Rad) and 50 mM dithiothreitol, heated to 37°C for 10 min, resolved in a 13% polyacrylamide gel, and transferred onto PVDF membranes (Immobilon PVDF; Millipore) for immunoblot analysis.

2.12 Western blot and densitometry analysis

After transfer, the membranes containing the blotted proteins were blocked and incubated with primary antibodies diluted as described in the Antibodies section. After washing, the membranes were incubated with peroxidase-conjugated secondary antibodies and washed again. Reactive proteins were revealed with an enhanced chemiluminescent detection system (ECL-Plus; Pierce Euroclone) and visualized on a VersaDoc imaging system (Bio-Rad). Images were analyzed using ImageJ software (National Institutes of Health, Bethesda, MD). For relative quantification, the optical density value was determined for equal-sized boxes that were drawn around antibody stained bands, and the background values were obtained below each band of interest to account for nonspecific antibody staining in the lane.

2.13 Coimmunoprecipitation

Protein lysates prepared as described previously were incubated overnight at 4°C on a mechanical rotator with anti-AQP4ex antibody or anti-Syntrophin antibody. The next day, 50 µL of prewashed agarose beads (rProteinG Agarose; Invitrogen) was added and incubated for 1 h at 4°C. Negative controls were set up by omitting the protein lysate or antibodies. To precipitate the immunocomplexes, the samples were centrifuged at 22,000 ×g at 4°C for 5 min and washed five times with washing buffer (0.2% Triton X-100, 10 mM Tris-HCl, pH 7.4, 150 mM NaCl, 1 mM EDTA, 1 mM ethylene glycol tetraacetic acid [EGTA]) plus Protease Inhibitor Cocktail. Proteins were eluted from the agarose beads by adding 50 µL of 2× Laemmli Sample Buffer and incubating at 37°C for 10 min. The eluted proteins were subjected to SDS-PAGE as previously described.

2.14 Statistical analysis

Statistical analyses were conducted using GraphPad Prism 4 software. All data are reported as the mean±*SEM*. We used Student's *t* test for unpaired data and analysis of variance for multiple statistical comparisons between groups. Differences were considered significant only for $p<.05$. No statistical methods were used to predetermine the sample sizes, but our sample sizes are similar to those generally employed in the field and are indicated in the figure legends.

3 Results

3.1 AQP4ex expression and localization in tissues

As a first step to assess the physiological significance of the extended AQP4 isoform, expression in human skeletal muscle and in the central nervous system (CNS) was investigated by immunofluorescence and immunoblotting. To perform this analysis, we used an anti-AQP4ex antibody that was specifically produced against a unique peptide (DRTESRQDSLELSS) located within the predicted AQP4 readthrough extension (Figure 1a). Immunolocalization of AQP4 isoforms in human biopsies (Figure 1b) revealed expression of the AQP4ex isoform in the spinal cord, particularly in astrocyte processes of the external layers of white matter; the central gray matter appeared not stained compared with the staining of canonical AQP4. AQP4ex expression was also observed in pericapillary astrocyte endfeet. In skeletal muscle, the expression of AQP4ex was still confined at the sarcolemma although its immunofluorescence signal appeared weaker. Immunoblotting analysis using anti-AQP4 antibodies with human extracts revealed the classical two major bands (32 and 30 kDa), which corresponded to AQP4-M1 and AQP4-M23, and two less commonly detected bands (38 and 35 kDa), which were specifically revealed with the AQP4ex-Ab, indicating that they corresponded to AQP4-M1ex and AQP4-M23ex (Figure 1c). Native 2DE (BN/SDS-PAGE) with brain extract revealed that AQP4ex was mainly confined to the high-molecular-size AQP4 pools (Supporting Information Figure S1). Densitometric analysis revealed that the relative abundance of AQP4ex compared with total AQP4 was approximately 10% in the CNS and 40% in the skeletal muscle (Figure 1d). A more detailed tissue distribution analysis was performed in rat using species-specific AQP4ex antibodies. Immunofluorescence analysis confirmed that AQP4ex was also expressed in rat, exhibiting similar tissue expression and distribution levels to those observed in humans (Supporting Information Figure S2). In particular, the selective perivascular expression of AQP4ex was better evaluated in the cerebellum. These results confirm that AQP4 translational readthrough occurs in vivo in both humans and in the rat, and suggest that AQP4ex could have a more selective location than AQP4 in the same tissues.

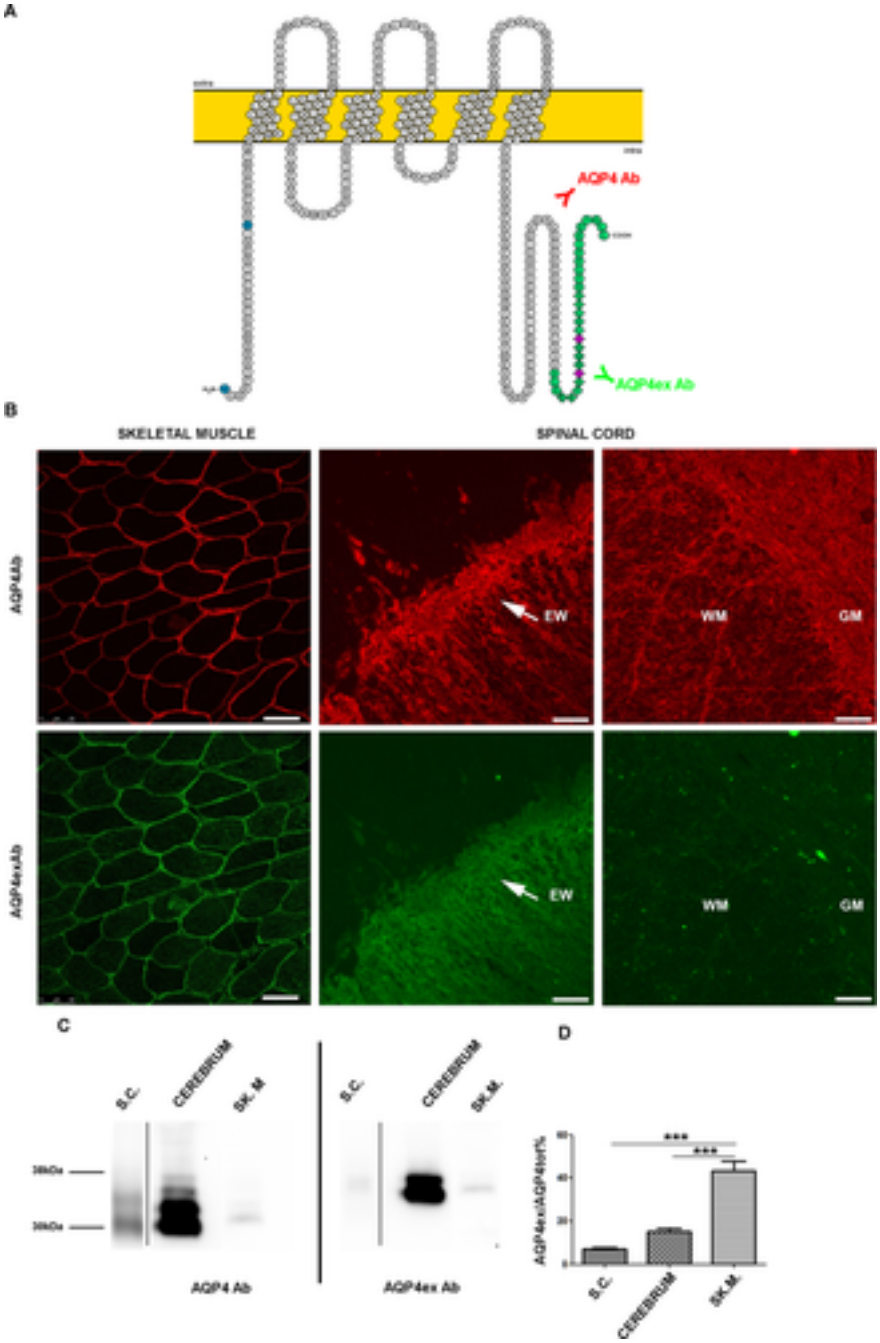

Figure 1

AQP4ex is a novel isoform of AQP4 that is expressed in human tissues. (a) Representation of the primary amino acid sequence and membrane topology of extended aquaporin 4 (AQP4ex). The two translation initiation sites, Met1 and Met23, corresponding to the two canonical AQP4 isoforms, M1 and M23, respectively, are highlighted in blue. The amino acid C-terminal extension is represented in green. The extended isoform shows two serines (in magenta) within the putative consensus phosphorylation (RXXS) motif. The commercial anti-AQP4 antibody is represented in red near the recognized epitope, whereas the anti-AQP4ex antibody is represented in green, and the specific recognized epitope is represented as a rhombus. (b) Distribution of the AQP4 (red) and AQP4ex (green) isoforms in human skeletal muscle and spinal cord biopsies. Scale bar = 50 µm. (c) Immunoblot detection of AQP4 isoforms expressed in human cerebrum, spinal cord (S.C.) and skeletal muscle (SK.M.). Four bands of 32, 30, 38, and 35 kDa were detected that corresponded to AQP4-M1, AQP4-

M23, AQP4-M1ex, and AQP4-M23ex, respectively. Tissues lysates were probed with anti-AQP4 and anti-AQP4ex antibodies. (d) Histogram showing the percentage of AQP4ex relative to the total AQP4 measured by human tissue immunoblotting (***$p < .0001$, $n = 5$). EW, external white matter; WM, white matter; GM, gray matter [Color figure can be viewed at wileyonlinelibrary.com]

3.2 Natural context and regulation of AQP4-TRT

To investigate the mechanism and regulation of AQP4-TRT, we first analyzed the frequency of this phenomenon in a transfected cell model. To achieve this goal, we cloned AQP4-CDS with its 3'UTR sequence up to the second stop codon (AQP4-3'UTR) and analyzed AQP4 isoform expression. The major isoforms detected were, as expected, AQP4-M1 and AQP4-M23. To a lesser extent, two other longer AQP4 isoforms with a length of 35 kDa and 38 kDa were also detected. These two additional proteins corresponded to the extended AQP4 proteins, as confirmed by the use of the specific anti-AQP4ex antibody (Figure 2a). Densitometric analysis showed that the extended isoforms, generated by readthrough in this experimental condition, constituted approximately 10% of all AQP4 isoforms.

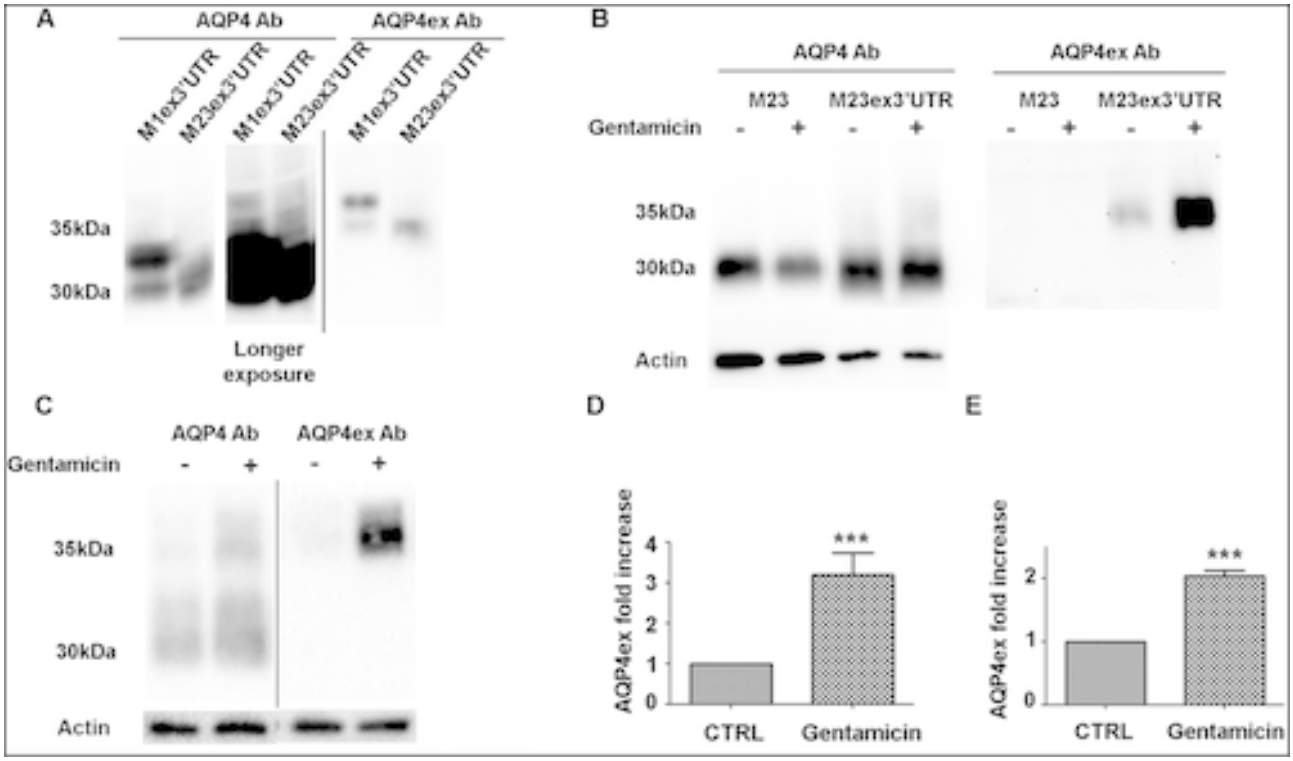

Figure 2

AQP4ex is generated by programmed translational readthrough. (a) Immunoblot showing the efficiency of AQP4 programmed translational readthrough in vitro. In the M1ex 3'UTR and M23ex 3'UTR transfected cells, anti-AQP4 antibody recognized two bands of 32 and 30 kDa, which were related to AQP4-M1 and AQP4-M23. A longer exposure revealed two more weak bands at 35 kDa and 38 kDa that were related to AQP4-M1ex and AQP4-M23ex, as confirmed by the detection of two proteins of the same size by the anti-AQP4ex antibody. (b) Immunoblot showing the effect of 24 h of gentamicin treatment on AQP4 translational readthrough in transiently transfected U87 cells (c) and in primary rat astrocyte cell cultures. (d, e) Densitometric analysis of the expression levels of AQP4ex,

relative to the total AQP4, after gentamicin treatment in U87-transfected cells (d) and in primary rat astrocytes cell cultures (e). Data are expressed as the means ± *SEM* of three independent experiments (Student's *t* test ***$p < .0003$)

As previously reported, aminoglycoside antibiotics such as gentamicin and G418 are known to result in the misreading of termination codons, thus enhancing the level of ribosomal readthrough (Martin, Mogg, Heywood, Nitschke, & Burke, 1989). Furthermore, the efficiency by which aminoglycosides confer readthrough strongly depends on the nucleotides flanking the stop codon. Therefore, to investigate to what extent this mechanism can occur, cells were transiently transfected with AQP4-3'UTR, and the effect of gentamicin treatment for 24 h on AQP4 protein expression was assessed. Interestingly, gentamicin induced a strong, three-fold increase in AQP4ex protein expression, whereas the protein expression of AQP4 remained unaffected (Figure 2b–d). Importantly, this positive modulation also occurred in rat astrocyte primary cell cultures, which exhibit high expression levels of endogenous AQP4 (Figure 2c–e). These results indicate that AQP4ex is produced by TRT and that the expression levels can be efficiently modulated.

3.3 AQP4ex characterization in vitro: Expression, localization, and supramolecular organization

Next, we evaluated the plasma membrane expression and supramolecular organization of AQP4ex. To achieve this goal, we generated two different AQP4 mutants in which the canonical stop codon, UGA, was replaced with the Trp-encoding UGG, ensuring efficient generation of the modified extended isoforms (AQP4-M1ex and AQP4-M23ex). First, we evaluated whether the C-terminal extension of the mutated isoforms influenced AQP4 protein expression. Using immunoblot analysis (Figure 3a), AQP4-M1ex resulted in the generation of two proteins that were specifically recognized by the AQP4ex antibody. These two proteins had the following predicted molecular weight: M1ex (38 kDa) and M23ex (35 kDa). Furthermore, M23ex was most likely generated by the LS mechanism, which is responsible for the generation of M23 from M1. These results demonstrated that the extended protein is produced at levels that are comparable to the canonical isoform and that the translational mechanisms, including LS, are not affected by the extended C-terminus. This finding further implies that a single M1 messenger transcript can produce four AQP4 isoforms.

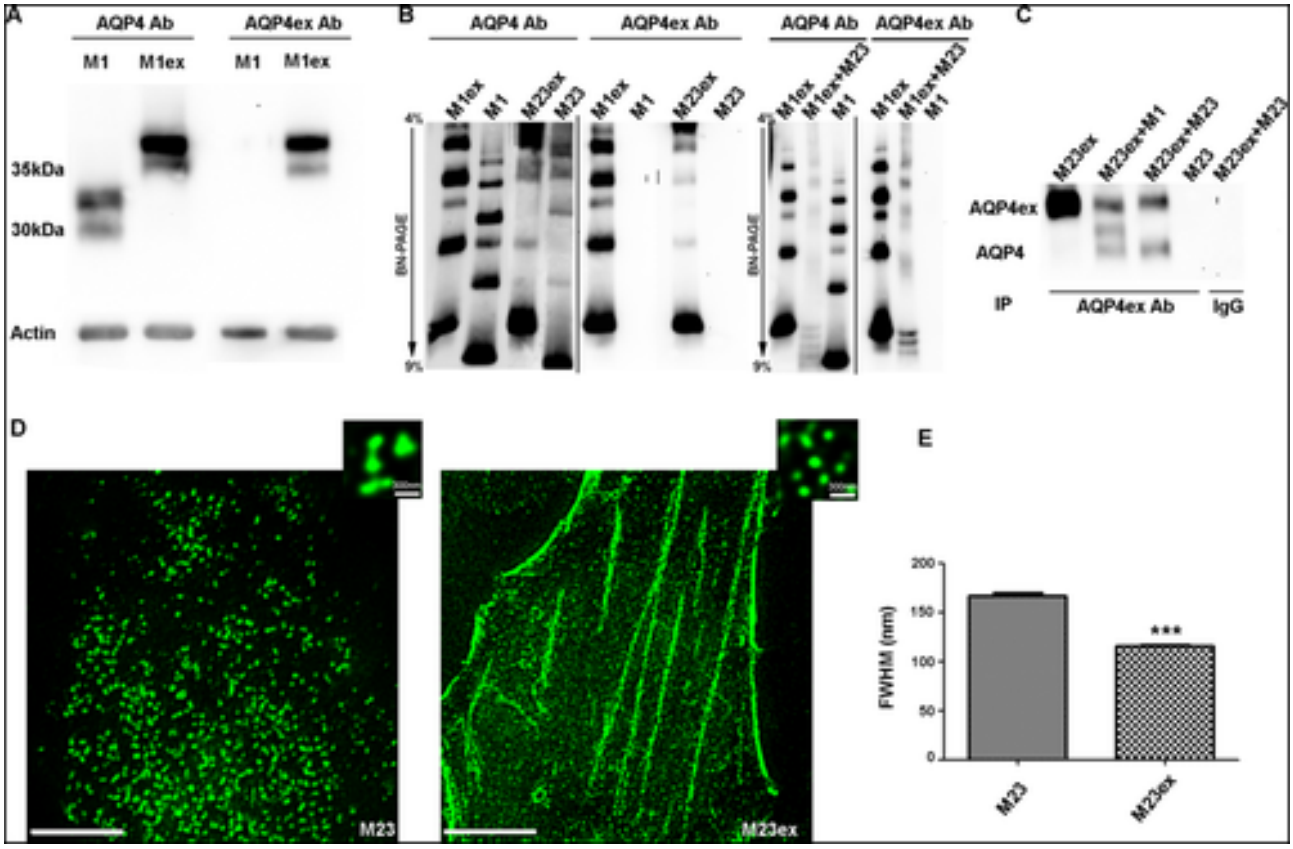

Figure 3

AQP4ex expression, etheroholigomerization and supramolecular organization. (a) Immunoblot detection of AQP4 and AQP4ex proteins in the U87 transfected cell line. In M1-transfected cells, the anti-AQP4 antibody recognized two bands at 32 and 30 kDa that were related to M1-AQP4 and M23-AQP4, respectively, whereas in U87 cells transfected with an M1-AQP4 mutant in which the canonical stop codon UGA was replaced by Trp-encoding UGG, two bands at 38 and 35 kDa were related to AQP4-M1ex and AQP4-M23ex, respectively. The anti-AQP4ex antibody specifically recognized exclusively AQP4-M1ex and AQP4-M23ex. Actin was used as a loading control. (b) Immunodetection by BN-PAGE of AQP4 pools in lysates obtained from U87 cells transfected with the canonical and the extended AQP4 isoforms alone or cotransfected in combination. BN-PAGE of lysates from transfected cells probed with anti-AQP4 and anti-AQP4ex antibodies. (c) U87 cells were cotransfected with the indicated expression constructs and lysates were immunoprecipitated with anti-AQP4ex or rabbit (immunoglobulin G) antibodies and subjected to immunoblot analysis with anti-AQP4 antibody. The top band corresponds to AQP4ex, and the bottom bands correspond to the canonical AQP4 isoforms. (d) AQP4 and AQP4ex-transfected cells were stained with anti-AQP4 antibody and imaged using STED microscopy as described in the Methods section. The inserts show a magnified view of the marked areas. Scale bars= 5 µm. (e) Histogram of the mean ± *SEM* of the cluster size of AQP4 measured based on the intensity profiles by full-width at half-maximal intensity (FWHM). At least 100 random clusters were measured from three different cells. Significance was tested using Student's *t* test, ***$p < .0001$ [Color figure can be viewed at wileyonlinelibrary.com]

It is well established that AQP4-M1 and AQP4-M23 form heterotetramers, which further aggregate into very well-ordered supramolecular structures (OAPs). To investigate the posttranslational

assembly of the extended isoforms and their correct targeting to the plasma membrane, cells were transfected with the AQP4 and AQP4ex isoforms and analyzed by BN-PAGE and confocal super-resolution microscopy (gSTED). The biochemical analysis showed that the extended isoforms aggregated into supramolecular structures comparable to those formed by the nonextended isoforms, although a shift was observed as consequence of the additional 29 amino acid extensions of each monomer (Figure 3b). Furthermore, cells that were co-transfected with both the short and the extended isoforms formed hybrid OAPs with an intermediate size compared to those formed by cells transfected with a single isoform. Co-immunoprecipitation experiments further confirmed that AQP4ex co-aggregated with the non-extended form (Figure 3c).

We subsequently employed gSTED microscopy to elucidate the arrangement of the AQP4 and AQP4ex at the nanometer scale (Figure 3d). Cells expressing only the M23ex isoform displayed clusters of OAPs that were significantly smaller, more homogenous in size and often arranged in a linear pattern compared to those formed by M23 alone. This result suggested that the C-terminal extension plays a role in determining the size of AQP4 clusters, thus limiting the number of tetramers that can be added to the forming OAPs.

3.4 AQP4ex polarization and interaction with α-syntrophin

In the CNS, AQP4 is expressed in pericapillary astrocyte processes and the glia limitans interna and externa. To determine whether AQP4ex is differentially expressed, we evaluated expression levels by immunofluorescence in the rat cerebrum and cerebellum. Interestingly, AQPex staining was much stronger in the pericapillary astrocyte endfeet compared with the other regions (Figure 4a). To better analyze this particular feature, we evaluated the expression of AQP4ex in the cerebellum, in which dystrophin-dependent (perivascular) and -independent pools of AQP4 have been described (Nicchia et al., 2008b). The expression of AQP4 was mainly localized to perivascular astrocyte processes, while the dense network of astrocyte processes in the granular layer displayed much less staining, indicating that AQP4ex might interact with the dystrophin complex at the perivascular pole (Figure 4a). The 2DE experiments indicated that AQP4ex is enriched in high-molecular weight pools of AQP4 (Figure 4b), which have been demonstrated to be dependent on dystrophin (Nicchia, Rossi, Nudel, Svelto, & Frigeri, 2008c). Previous studies have suggested that AQP4 may interact with α-syntrophin in both the CNS (Neely et al., 2001) and the skeletal muscle (Frigeri et al., 2002). Furthermore, α-syntrophin-KO mice display mislocalization of AQP4 (Amiry-Moghaddam et al., 2003). To determine whether AQP4ex interacts with α-syntrophin, cell transfection and immunoprecipitation experiments were performed. In transfected cells, AQP4ex and α-syntrophin largely co-localized at the plasma membrane, while the canonical form showed no co-localization (Figure 4c). Furthermore, AQP4ex showed high levels of co-purification with α-syntrophin in co-IP experiments, indicating an effective interaction of the two proteins (Figure 4d). Considered together, these data show that AQP4ex at the perivascular pole interacts with the dystrophin complex throughout α-syntrophin.

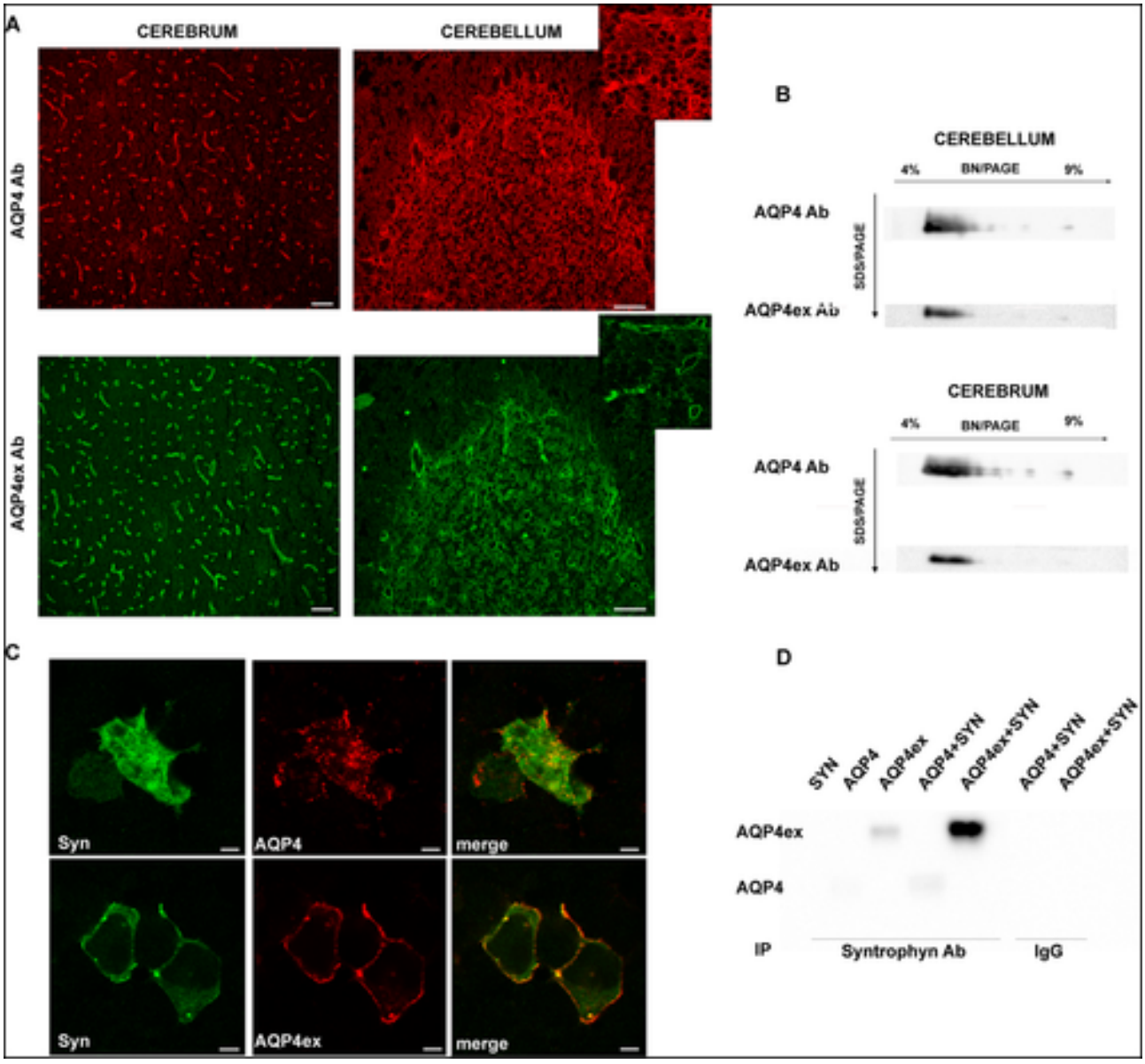

Figure 4

AQP4ex polarization and interaction with the DGC complex. (a) Localization of AQP4 (red) and AQP4ex (green) isoforms in rat cerebrum and cerebellum analyzed by confocal microscopy. Scale bar = 50 μm. (b) Immunodetection of AQP4 and AQP4ex pools in the rat cerebrum and cerebellum after 4 to 9% gradient BN-PAGE and 13% SDS-PAGE. (c) Confocal image showing the localization of AQP4 or AQP4ex (red) and syntrophyn (green) in transfected HEK cells. Note the colocalization of the extended isoform with syntrophin. The images are representative of six independent experiments. Scale bar = 10 μm. (d) The cells were cotransfected with the indicated expression constructs, and the lysates were immunoprecipitated with anti-syntrophin or rabbit (immunoglobulin G) antibodies and subjected to immunoblot analysis with anti-AQP4 antibody. The top band corresponds to AQP4ex, and the bottom bands correspond to the canonical AQP4 isoform [Color figure can be viewed at wileyonlinelibrary.com]

3.5 AQP4ex functional characterization: Water transport capability

To acquire insight into the functional significance of AQP4ex, water transport properties were investigated using two different functional assays. The membrane expression levels of the proteins were evaluated by immunofluorescence and Western blot analysis. The fluorescence quenching-based assay was used to measure the kinetics of volume changes of transfected cells after osmotic shock, revealing high levels of water transport via AQP4ex in transfected cells that were similar to those of AQP4-transfected cells (Figure 5a). The oocyte-swelling assay was performed to measure the osmotic permeability coefficient. AQP4 and AQP4ex oocytes analyzed 48 h after cRNA injection displayed a similar three-fold increase in Pf compared with the control injected oocytes, indicating that the water transport properties of AQP4ex were not substantially changed by the extended C-terminus (Figure 5b).

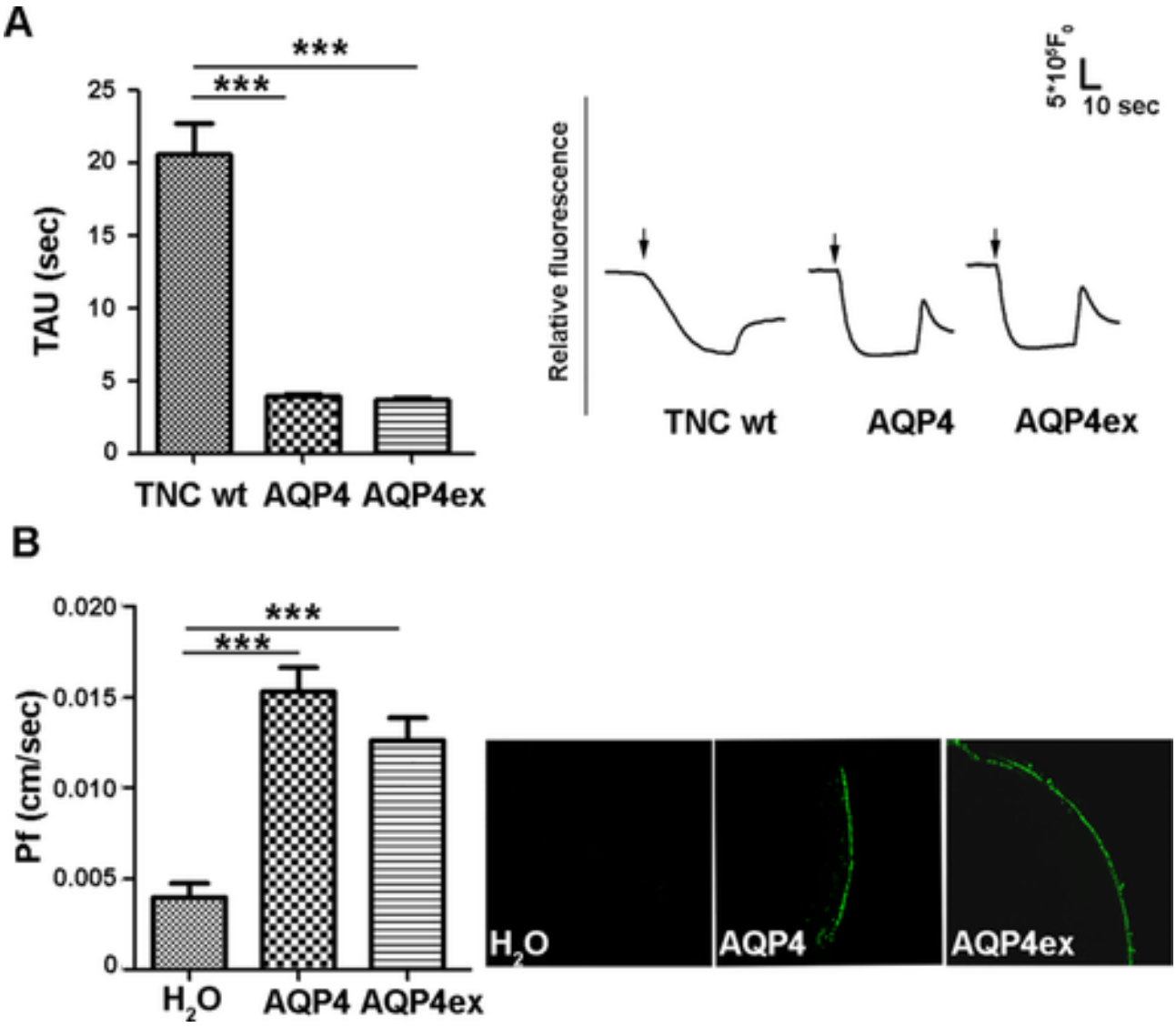

Figure 5

Water transport properties of the AQP4ex isoform. (a) Left, Histogram showing the mean±*SEM* values of time constants (tau) obtained by fitting an exponential curve to the cell shrinkage phase of cells after exposure to hypertonic solution (***$p<.0001$; $n=4$). Right, Representative time course of water transport recorded from TNC wt and stably transfected AQP4

and AQP4ex TNC cell lines performed with the Calcein-AM quenching assay. Arrows indicate the addition of a mannitol solution to PBS to achieve a final osmolarity of 450 mOsm. (b) Left, Histogram showing the mean±*SEM* of the corresponding P_f value. (*$p < .005$ vs. injected H_2O, $n = 10$). Right, AQP4 immunofluorescence analysis of *X. laevis*oocytes injected with water (H_2O), AQP4 cRNA, or AQP4ex cRNA. [Color figure can be viewed at wileyonlinelibrary.com]

3.6 New putative functional role of AQP4ex: Effect of phosphorylation

Different reports have demonstrated that TRT provides an important means by which genes acquire new functions throughout the course of evolution. In the case of AQP4ex, the C-terminal extension can alter protein stability, localization, and/or activity. The identification of exclusive novel signals in AQP4 readthrough extensions could help to unravel the role of this new isoform. Therefore, we screened the extended amino acid sequence to identify possible elements that could confer functional differences between the normal and the extended form of the AQP4 protein. The sequence was analyzed for the presence of endoplasmic retention signals, glycosylation, palmitoylation, and phosphorylation sites. An initial analysis with NetPhos2.0 revealed the presence of two serines (Ser331 and Ser335) within a high-score putative consensus phosphorylation (RXXS) motif. To gain insight into the effects of phosphorylation on the predictable serine residues, two double mutants of AQP4ex were generated in which Ser331 and Ser335 were replaced with alanines (AQP4exAla mutant) to prevent phosphorylation and with aspartates (M23exAsp mutant) in an attempt to mimic a phosphorylated serine. AQP4 immunolocalization showed that the mutation did not affect protein expression and did not impact correct plasma membrane targeting of AQP4 (Figure 6a). Interestingly, the AQP4exAsp mutant displayed well-ordered linear staining similar to that occasionally observed for AQP4ex, whereas AQP4exAla showed a more diffuse staining similar to the AQP4 staining. Protein expression and OAP formation evaluated by 2DE (BN/SDS-PAGE) confirmed that there were no major changes between the two mutants (Supporting Information Figure S3). gSTED super-resolution microscopy in cells expressing the two mutants indicated that both AQP4exAla and AQP4exAsp formed OAPs with a size comparable to those of APQ4ex (Figure 6b).

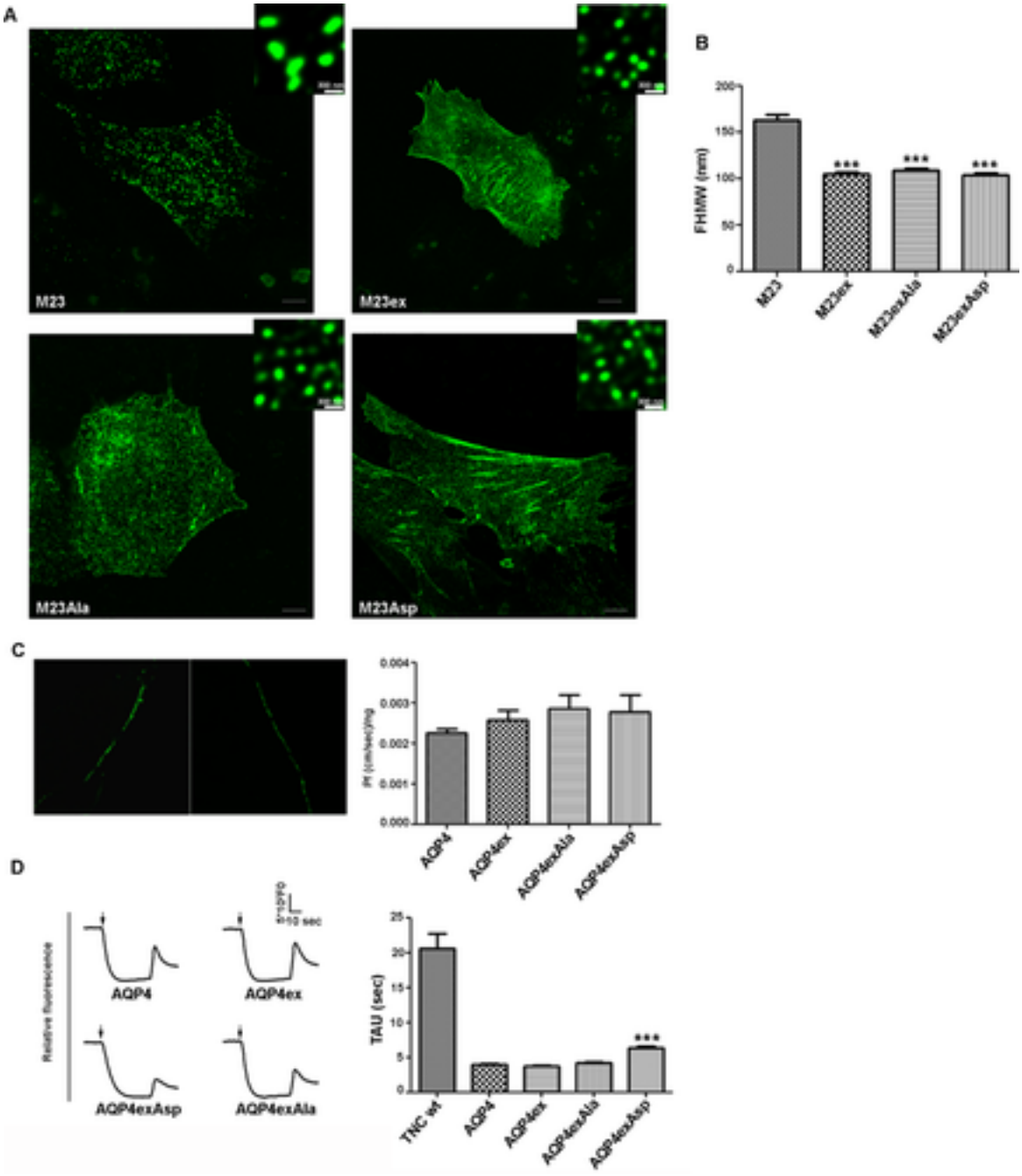

Figure 6

Phosphorylation on Ser residues in the AQP4ex extension does not affect the supramolecular organization of AQP4ex but affects AQP4-dependent cell water permeability. (a) AQP4, AQP4ex, AQP4exAla, and AQP4exAsp-transfected cells were stained with anti AQP4 antibody and imaged by STED microscopy as described in the Methods section. Scale bars =5 µm. The inserts show a magnified view of the marked areas. (b) Histogram showing the mean±*SEM*cluster size of AQP4 based on the intensity profiles by full-width at half-maximal intensity (FWHM). At least 100 random clusters were measured in at least four different cells. Significance was tested using Student's *t* test, ***$p < .0001$ compared with M23. (c) Left, AQP4 immunofluorescence analysis of *X. laevis*oocytes injected with AQP4exAla cRNA and AQP4exAsp cRNA. Right, Histogram showing the mean±*SE* of the corresponding P_f value (n = 15). (d) Left, Representative recording of changes in calcein fluorescence observed in response to hyperosmotic shock in AQP4, AQP4ex, AQP4exAla, or AQP4exAsp-

transfected TNC cells. Arrows indicate the addition of mannitol solution to PBS to achieve a final osmolarity of 450 mOsm. Right, Histogram showing the means±*SEM* values of time constants (tau) (*n* = 6, ***$p < .0001$) [Color figure can be viewed at wileyonlinelibrary.com]

To gain insight regarding the role played by Ser331 and Ser335 in the regulation of AQP4 water channel function, water transport was evaluated in AQP4ex mutants. As shown in Figure 6c, the oocyte-swelling assay demonstrated that there were no substantial differences in the water transport properties of the two mutants compared with AQP4ex under the present experimental conditions, indicating that the mutation per se does not affect the water transport properties of AQP4ex. However, in stable transfected cell lines, the fluorescence quenching-based assay showed a reduction of water transport in cells expressing constitutively phosphorylated AQP4ex compared with all other isoforms (Figure 6d,e). No effect on water transport was observed in the AQP4exAla mutants, indicating that other cellular components may intervene to modulate AQPex activity in mammalian cells and suggesting that the two serines in the extended C-terminus of AQP4 play a role in modulating short-term water transport.

4 Discussion

In the present study, we describe two supplementary AQP4 isoforms that are generated by TRT.

Although readthrough events have been described in vertebrates, the functional significance of the readthrough product has not been shown. Two examples have been described to date. TRT of lactate dehydrogenase produces a peroxisome-specific novel isoform with a new function compared with the canonical cytosolic protein. More importantly, in VEGFA, a TRT event has been demonstrated to generate the anti-angiogenic isoform VEGF-Ax (Eswarappa et al., 2014).

Here, we present a new situation of a mammalian protein that is predominantly expressed in the astrocytes of the CNS and that can be generated by TRT; the extended form also has alternate functions compared with the shorter, canonical forms. The extended tail of the C-terminus of AQP4 has at least two structural/functional consequences. First, the extended portion restricts the size of the AQP4 clusters that can be formed. Indeed, while M23 is able to form large AQP4 suprastructures (OAPs) in transfected cells, under the same conditions, M23ex forms much smaller OAPs in the plasma membrane. Furthermore, these OAPs appear to be more homogeneous in size compared with those formed by M23, which instead can be very large. These findings indicate that the extended portion has an intrinsic capacity to limit the maximal size of OAPs by regulating the number of associated AQP4 tetramers. Thus, while extension at the N-terminus impairs the formation of OAPs, a similar extension at the C-terminus finely refines the formation of OAPs. This process results in the formation of OAPs that depend not only on the presence and amount of the M1 isoform but also on the presence and amount of the C-terminal extension. Our data highlight how AQP4 represents an excellent example of optimization of the genetic information and biological plasticity of the cell. In fact, both leaky scanning and readthrough coexist on the same AQP4 mRNA molecule and appear to be coordinated processes that enable the cell to produce four different protein isoforms starting

from a single AQP4 mRNA molecule. Interestingly, the coexistence of these mechanisms on the same transcript allows the cell to reduce (by leaky scanning) or extend (by readthrough) the length of the AQP4 protein by approximately the same length. This phenomenon was not only important for the behavior of the single protein itself but it also influenced the AQP4 supramolecular organization in OAPs by modifying their dimensions.

Our findings are important because it has been speculated that OAPs with a variable size have tissue-specific roles and are associated with different anchoring proteins (DGC or actin) (Nicchia et al., 2008a). Moreover, OAPs are involved in different neuromuscular diseases, such as Duchenne muscular dystrophy and NMO. Therefore, AQP4ex could be the "hidden player" that could have a crucial role in these physiopathological conditions. Interestingly, the expression of AQP4ex was strongly confined to perivascular astrocyte processes, indicating that, in this particular location, AQP4ex, likely in association with the canonical AQP4, constitutes the dystrophin-dependent perivascular pool of AQP4, which has been described in previous studies (Nicchia et al., 2008c). This was confirmed by demonstrating that α-syntrophin co-localizes and co-purifies with AQP4ex and not with the canonical AQP4. Remarkably, the canonical C-terminal SSV-motif of AQP4, assumed to interact with α-syntrophin through the PDZ-domain, is no more localized at the extreme C-terminal region of AQP4ex protein, suggesting that this particular location could be not essential for the interaction with α-syntrophin. Interestingly, several studies report that some PDZ domains could also bind to internal sequence of target proteins (Brenman et al., 1996; Wong et al., 2003). For example, the PDZ domain of the α-syntrophin has been reported to interact with an internal domain of the nNOS protein (Hillier, Christopherson, Prehoda, Bredt, & Lim, 1999). Therefore, a similar interaction could be hypothesized for AQP4ex and α-syntrophin. Another possibility is that other c-terminal amino acids, alone or in combination with the internal SSV motif of AQP4ex, may be involved α-syntrophin interaction.

Our data suggest that AQP4ex may be directly involved in the alteration of the BBB observed when the dystrophin complex is altered, such as in the dystrophin-deficient (Frigeri et al., 2002) or in α-syntrophin-null mice (Neely et al., 2001). Loss of AQP4 polarization at perivascular membrane is also reported in different pathological state, such as epilepsy (Alvestad et al., 2013; Eid et al., 2005), traumatic brain injury (Ren et al., 2013), stroke (Frydenlund et al., 2006), and in Alzheimer disease (Yang et al., 2011; Zeppenfeld et al., 2016) and was often associated with impairment of perivascular-interstitial fluid exchange and interstitial solutes clearance; however, the mechanisms involved are poorly understood. Our discovery that AQP4ex is mainly localized at the perivascular level adds complexity to the concept of astrocyte polarization and highlights a possible involvement of these isoforms in such pathological states and may pave the way for a more complete mechanistic understanding of AQP4 polarization loss in diseases.

Interestingly, we provide evidence that phosphorylation may play a crucial role in AQP4ex water transport, adding another potential key point regarding AQP4 regulation. Indeed, mutagenesis

experiments demonstrated that the modification of two potentially phosphorylatable serines in the AQP4 extension resulted in a reduction of the membrane water permeability with a concomitant change in the plasma membrane assembly of AQP4ex. Although phosphorylation-dependent gating of AQP4 has been proposed as a regulatory mechanism for AQP4-mediated osmotic water transport, all of these studies were performed using the canonical form of AQP4 and are related to other serines in the AQP4 sequence (Assentoft et al., 2013; Madrid et al., 2001; Zelenina et al., 2002). Moreover, phosphorylation of the AQP4ex residues may be involved in the regulated osmo-sensitive vesicular trafficking of aquaporin to the plasma membrane as it has been suggested for AQP4 and AQP1 (Conner et al., 2012; Kitchen et al., 2015).

It has been estimated that the level of basal readthrough of stop codons in mammalian cells ranges from 0.01 to 0.1%. However, AQP4ex represents a significant amount (approximately 10%) of the total AQP4 in the CNS tissue, and even higher levels are found in skeletal muscle. This could be due to the he UGA stop codon, which has the highest basal RT potential (Beier & Grimm, 2001) and to programmed readthrough that allows the attainment of very high levels. The latter suggests that AQP4ex expression may undergo regulation under physiological or pathological conditions, as confirmed by the effect of aminoglycoside antibiotics on AQP4 readthrough. In fact, both in transfected cells and rat astrocyte primary cell cultures, gentamicin treatment induced a remarkable increase in AQP4ex expression. As a consequence, common pharmacological treatment with aminoglycoside antibiotics should result in an increase in AQP4ex expression.

Our findings shed light on the composite regulation of AQP4 expression, in which translational readthrough, together with alternative splicing, leaky scanning, and reinitiation mechanisms, contribute to the dynamic regulation of the expression of AQP4 isoforms and OAP formation. These tissue-specific posttranscriptional regulatory mechanisms superimpose fine-tuning control upon on–off switches that are characteristic of gene transcription and may have physiopathological implications under conditions in which AQP4 and/or OAP alterations have been reported, such as those related to astrocyte cell migration (i.e., glia scar formation) as well as those involving AQP4 supramolecular organization or function such as neuromyelitis optica. Finally, this new isoform, together with the two major isoforms M1 and M23, may inhabit the same cell, with the resulting phenotype representing a balance between their expression levels.

In conclusion we show that AQP4 mRNA undergoes programmed translational readthrough to generate AQP4ex, a new isoform that contains a unique C-terminal extension. This extended isoform is widely expressed in human tissues, and high expression levels correlate with smaller OAPs in comparison with the canonical ones. The extended C-terminus exhibits several domains that could be involved in AQP4 regulation, leading us to speculate that this isoform has an important regulatory role in OAP assembly and stability.

Acknowledgment

The authors thank Dr. Gary Loughran for the kind gift of anti-AQP4ex antibody, Mr. Gaetano De Vito for his excellent technical assistance and Dr. Adrea Rossi for discussion. This study was financed by the Italian Ministry of University and Research (Project Firb “Futuro in Ricerca” RBFR12SJA8 to Grazia Paola Nicchia, by Apulian Region funding PON project 01_01297 to Antonio Frigeri and by Apulian Region funding PON project 02_00576_3329762 “AMIDHERA-Sistemi avanzati mini-invasivi di diagnosi e radioterapia” to Maria Svelto. Dr. Francesco Pisani is a research fellow of the Apulia region program “Future in research” (project n. 5CU9HC5).

References

- Alvestad, S., Hammer, J., Hoddevik, E. H., Skare, O., Sonnewald, U., Amiry-Moghaddam, M., & Ottersen, O. P. (2013). Mislocalization of AQP4 precedes chronic seizures in the kainate model of temporal lobe epilepsy. Epilepsy Research, 105, 30– 41.

  CrossrefCASPubMedWeb of Science®Google Scholar

- Amiry-Moghaddam, M., Otsuka, T., Hurn, P. D., Traystman, R. J., Haug, F. M., Froehner, S. C., … Bhardwaj, A. (2003). An alpha-syntrophin-dependent pool of AQP4 in astroglial end-feet confers bidirectional water flow between blood and brain. Proceedings of the National Academy of Sciences of the United States of America, 100, 2106– 2111.

  CrossrefCASPubMedWeb of Science®Google Scholar

- Assentoft, M., Kaptan, S., Fenton, R. A., Hua, S. Z., de Groot, B. L., & MacAulay, N. (2013). Phosphorylation of rat aquaporin-4 at Ser(111) is not required for channel gating. Glia, 61, 1101– 1112.

  Wiley Online LibraryCASPubMedWeb of Science®Google Scholar

- Beier, H., & Grimm, M. (2001). Misreading of termination codons in eukaryotes by natural nonsense suppressor tRNAs. Nucleic Acids Research, 29, 4767– 4782.

  Google Scholar

- Brenman, J. E., Chao, D. S., Gee, S. H., McGee, A. W., Craven, S. E., Santillano, D. R., … Bredt, D. S.(1996). Interaction of nitric oxide synthase with the postsynaptic density protein PSD-95 and alpha1-syntrophin mediated by PDZ domains. Cell, 84, 757– 767.

  CrossrefCASPubMedWeb of Science®Google Scholar

- Conner, M. T., Conner, A. C., Bland, C. E., Taylor, L. H., Brown, J. E., Parri, H. R., & Bill, R. M. (2012). Rapid aquaporin translocation regulates cellular water flow: Mechanism of hypotonicity-induced subcellular localization of aquaporin 1 water channel. Journal of Biological Chemistry, 287, 11516– 11525.

  CrossrefCASPubMedWeb of Science®Google Scholar

- De Bellis, M., Pisani, F., Mola, M. G., Basco, D., Catalano, F., Nicchia, G. P., … Frigeri, A. (2014). A novel human aquaporin-4 splice variant exhibits a dominant-negative activity: A new mechanism to regulate water permeability. Molecular Biology of the Cell, 25, 470– 480.

  CrossrefCASPubMedWeb of Science®Google Scholar

- Dunn, J. G., Foo, C. K., Belletier, N. G., Gavis, E. R., & Weissman, J. S. (2013). Ribosome profiling reveals pervasive and regulated stop codon readthrough in Drosophila melanogaster. Elife, 2, e01179.

  CrossrefPubMedWeb of Science®Google Scholar

- Eid, T., Lee, T. S., Thomas, M. J., Amiry-Moghaddam, M., Bjornsen, L. P., Spencer, D. D., … de Lanerolle, N. C. (2005). Loss of perivascular aquaporin-4 may underlie deficient water and K+ homeostasis in the human epileptogenic hippocampus. Proceedings of the National Academy of Sciences of the United States of America, 102, 1193– 1198.

  CrossrefCASPubMedWeb of Science®Google Scholar

- Eswarappa, S. M., Potdar, A. A., Koch, W. J., Fan, Y., Vasu, K., Lindner, D., … Fox PL. (2014). Programmed translational readthrough generates antiangiogenic VEGF-Ax. Cell, 157, 1605– 1618.

  CrossrefCASPubMedWeb of Science®Google Scholar

- Frigeri, A., Nicchia, G. P., Repetto, S., Bado, M., Minetti, C., & Svelto, M. (2002). Altered aquaporin-4 expression in human muscular dystrophies: A common feature? FASEB Journal, 16, 1120– 1122.

  Wiley Online LibraryCASPubMedWeb of Science®Google Scholar

- Frydenlund, D. S., Bhardwaj, A., Otsuka, T., Mylonakou, M. N., Yasumura, T., Davidson, K.G., … Amiry-Moghaddam, M. (2006). Temporary loss of perivascular aquaporin-4 in neocortex after transient middle cerebral artery occlusion in mice. Proceedings of the National Academy of Sciences of the United States of America, 103, 13532– 13536.

  CrossrefCASPubMedWeb of Science®Google Scholar

- Han, Z., Wax, M. B., & Patil, R. V. (1998). Regulation of aquaporin-4 water channels by phorbol ester-dependent protein phosphorylation. Journal of Biological Chemistry, 273, 6001– 6004.

  CrossrefCASPubMedWeb of Science®Google Scholar

- Hillier, B. J., Christopherson, K. S., Prehoda, K. E., Bredt, D. S., Lim, W. A. (1999). Unexpected modes of PDZ domain scaffolding revealed by structure of nNOS-syntrophin complex. Science, 284, 812– 815.

  CrossrefCASPubMedWeb of Science®Google Scholar

- Jalajakumari, M. B., Manning, P. A. (1989). Nucleotide sequence of the traD region in the Escherichia coli F sex factor. Gene, 81, 195– 202.

  CrossrefCASPubMedWeb of Science®Google Scholar

- Kitchen, P., Day, R. E., Taylor, L. H., Salman, M. M., Bill, R. M., Conner, M. T., Conner, A. C. (2015). Identification and molecular mechanisms of the rapid tonicity-induced relocalization of the aquaporin 4 channel. Journal of Biological Chemistry, 290, 16873– 81.

  CrossrefCASPubMedWeb of Science®Google Scholar

- Lennon, V. A., Kryzer, T. J., Pittock, S. J., Verkman, A. S., Hinson, S. R. (2005). IgG marker of optic-spinal multiple sclerosis binds to the aquaporin-4 water channel. Journal of Experimental Medicine, 202, 473– 477.

  CrossrefCASPubMedWeb of Science®Google Scholar

- Li, G. P., Rice, C. M. (1989). Mutagenesis of the in-frame opal termination codon preceding nsP4 of Sindbis virus: Studies of translational readthrough and its effect on virus replication. Journal of Virology, 63, 1326– 1337.

  CrossrefCASPubMedWeb of Science®Google Scholar

- Loughran, G., Chou, M. Y., Ivanov, I. P., Jungreis, I., Kellis, M., Kiran, A. M., … Atkins, J. F. (2014). Evidence of efficient stop codon readthrough in four mammalian genes. Nucleic Acids Research, 42, 8928– 8938.

  CrossrefCASPubMedWeb of Science®Google Scholar

- Madrid, R., Le Maout, S., Barrault, M. B., Janvier, K., Benichou, S., & Merot, J. (2001). Polarized trafficking and surface expression of the AQP4 water channel are coordinated by serial and regulated interactions with different clathrin-adaptor complexes. EMBO Journal, 20, 7008– 7021.

  Wiley Online LibraryCASPubMedWeb of Science®Google Scholar

- Martin, R., Mogg, A. E., Heywood, L. A., Nitschke, L., & Burke, J. F. (1989). Aminoglycoside suppression at UAG, UAA and UGA codons in Escherichia coli and human tissue culture cells. Molecular Genetics and Genomics, 217, 411– 418.

  CrossrefCASPubMedWeb of Science®Google Scholar

- McCoy, E. S., Haas, B. R., & Sontheimer, H. (2010). Water permeability through aquaporin-4 is regulated by protein kinase C and becomes rate-limiting for glioma invasion. Neuroscience, 168, 971– 981.

  CrossrefCASPubMedWeb of Science®Google Scholar

- Moe, S. E., Sorbo, J. G., Sogaard, R., Zeuthen, T., Petter Ottersen, O., & Holen, T. (2008). New isoforms of rat aquaporin-4. Genomics, 91, 367– 377.

  CrossrefCASPubMedWeb of Science®Google Scholar

- Mola, M. G., Nicchia, G. P., Svelto, M., Spray, D. C., & Frigeri, A. (2009). Automated cell-based assay for screening of aquaporin inhibitors. Analytical Chemistry, 81, 8219– 8229.

CrossrefCASPubMedWeb of Science®Google Scholar

- Namy, O., Duchateau-Nguyen, G., Hatin, I., Hermann-Le Denmat, S., Termier, M., & Rousset, J. P.(2003). Identification of stop codon readthrough genes in Saccharomyces cerevisiae. Nucleic Acids Research, 31, 2289– 2296.

CrossrefCASPubMedWeb of Science®Google Scholar

- Neely, J. D., Amiry-Moghaddam, M., Ottersen, O. P., Froehner, S. C., Agre, P., & Adams, M. E. (2001). Syntrophin-dependent expression and localization of Aquaporin-4 water channel protein. Proceedings of the National Academy of Sciences of the United States of America, 98, 14108– 14113.

CrossrefCASPubMedWeb of Science®Google Scholar

- Nicchia, G. P., Cogotzi, L., Rossi, A., Basco, D., Brancaccio, A., Svelto, M., & Frigeri, A. (2008a). Expression of multiple AQP4 pools in the plasma membrane and their association with the dystrophin complex. Journal of Neurochemistry, 105, 2156– 2165.

Wiley Online LibraryCASPubMedWeb of Science®Google Scholar

- Nicchia, G. P., Ficarella, R., Rossi, A., Giangreco, I., Nicolotti, O., Carotti, A., … Frigeri, A. (2011). D184E mutation in aquaporin-4 gene impairs water permeability and links to deafness. Neuroscience, 197, 80– 88.

CrossrefCASPubMedWeb of Science®Google Scholar

- Nicchia, G. P., Frigeri, A., Liuzzi, G. M., & Svelto, M. (2003). Inhibition of aquaporin-4 expression in astrocytes by RNAi determines alteration in cell morphology, growth, and water transport and induces changes in ischemia-related genes. FASEB Journal, 17, 1508– 1510.

Wiley Online LibraryCASPubMedWeb of Science®Google Scholar

- Nicchia, G. P., Mastrototaro, M., Rossi, A., Pisani, F., Tortorella, C., Ruggieri, M., … Svelto, M. (2009). Aquaporin-4 orthogonal arrays of particles are the target for Neuromyelitis optica autoantibodies. Glia, 57, 1363– 1373.

Wiley Online LibraryPubMedWeb of Science®Google Scholar

- Nicchia, G. P., Rossi, A., Mola, M. G., Procino, G., Frigeri, A., & Svelto, M. (2008b). Actin cytoskeleton remodeling governs aquaporin-4 localization in astrocytes. Glia, 56, 1755– 1766.

Wiley Online LibraryPubMedWeb of Science®Google Scholar

- Nicchia, G. P., Rossi, A., Nudel, U., Svelto, M., & Frigeri, A. (2008c). Dystrophin-dependent and -independent AQP4 pools are expressed in the mouse brain. Glia, 56, 869– 876.

Wiley Online LibraryCASPubMedWeb of Science®Google Scholar

- Papadopoulos, M. C., & Verkman, A. S. (2013). Aquaporin water channels in the nervous system. Nature Reviews Neuroscience, 14, 265– 277.

CrossrefCASPubMedWeb of Science®Google Scholar

- Pelham, H. R. (1978). Leaky UAG termination codon in tobacco mosaic virus RNA. Nature, 272, 469– 471.

CrossrefCASPubMedWeb of Science®Google Scholar

- Pisani, F., Mola, M. G., Simone, L., Rosito, S., Alberga, D., Mangiatordi, G. F., … Nicchia, G. P. (2015). Identification of a point mutation impairing the binding between aquaporin-4 and neuromyelitis optica autoantibodies. Journal of Biological Chemistry, 289, 30578– 30589.

CrossrefCASWeb of Science®Google Scholar

- Pisani, F., Rossi, A., Nicchia, G. P., Svelto, M., & Frigeri, A. (2011). Translational regulation mechanisms of aquaporin-4 supramolecular organization in astrocytes. Glia, 59, 1923– 1932.

Wiley Online LibraryPubMedWeb of Science®Google Scholar

- Ren, Z., Iliff, J. J., Yang, L., Yang, J., Chen, X., Chen, M. J., … Nedergaard, M. (2013). 'Hit & Run' model of closed-skull traumatic brain injury (TBI) reveals complex patterns of

posttraumatic AQP4 dysregulation. Journal of Cerebral Blood Flow and Metabolism 33, 834– 845.

CrossrefCASPubMedWeb of Science®Google Scholar

- Robinson, D. N., & Cooley, L. (1997). Examination of the function of two kelch proteins generated by stop codon suppression. Development, 124, 1405– 1417.

CASPubMedWeb of Science®Google Scholar

- Rossi, A., Pisani, F., Nicchia, G. P., Svelto, M., & Frigeri, A. (2010). Evidences for a leaky scanning mechanism for the synthesis of the shorter M23 protein isoform of aquaporin-4: implication in orthogonal array formation and neuromyelitis optica antibody interaction. Journal of Biological Chemistry, 285, 4562– 4569.

CrossrefCASPubMedWeb of Science®Google Scholar

- Schagger, H., Cramer, W. A., & von Jagow, G. (1994). Analysis of molecular masses and oligomeric states of protein complexes by blue native electrophoresis and isolation of membrane protein complexes by two-dimensional native electrophoresis. Analytical Biochemistry, 217, 220– 230.

CrossrefCASPubMedWeb of Science®Google Scholar

- Schueren, F., Lingner, T., George, R., Hofhuis, J., Dickel, C., Gartner, J., & Thoms, S. (2014). Peroxisomal lactate dehydrogenase is generated by translational readthrough in mammals. Elife, 3, e03640.

CrossrefPubMedWeb of Science®Google Scholar

- Wong, H. C., Bourdelas, A., Krauss, A., Lee, H. J., Shao, Y., Wu, D., … Zheng, J. (2003). Direct binding of the PDZ domain of dishevelled to a conserved internal sequence in the C-terminal region of Frizzled. Molecular Cell, 12, 1251– 1260.

CrossrefCASPubMedWeb of Science®Google Scholar

- Yang, J., Lunde, L. K., Nuntagij, P., Oguchi, T., Camassa, L. M., Nilsson, L. N., … Torp, R. (2011). Loss of astrocyte polarization in the tg-ArcSwe mouse model of Alzheimer's disease. Journal of Alzheimer's Disease, 27, 711– 722.

CrossrefCASPubMedWeb of Science®Google Scholar

- Zelenina, M., Zelenin, S., Bondar, A. A., Brismar, H., & Aperia, A. (2002). Water permeability of aquaporin-4 is decreased by protein kinase C and dopamine. American Journal of Physiology and Renal Physiology, 283, F309-F 318.

CrossrefCASPubMedWeb of Science®Google Scholar

- Zeppenfeld, D. M., Simon, M., Haswell, J. D., D'Abreo, D., Murchison, C., Quinn, J. F., … Iliff, J. J.(2016). Association of perivascular localization of aquaporin-4 with cognition and Alzheimer disease in aging brains. JAMA Neurology, 74, 91– 99.

CrossrefWeb of Science®Google Scholar

- Zuidscherwoude, M., Gottfert, F., Dunlock, V. M., Figdor, C. G., van den Bogaart, G., & van Spriel, A. B. (2015). The tetraspanin web revisited by super-resolution microscopy. Scientific Reports, 5, 12201.

CrossrefCASPubMedWeb of Science®Google Scholar